

November 2015

# Entanglement entropy in scalar field theory on the fuzzy sphere

Shizuka OKUNO<sup>1)\*</sup>, Mariko SUZUKI<sup>1,2)†</sup> AND Asato TSUCHIYA<sup>1,2)‡</sup>

<sup>1)</sup> *Department of Physics, Shizuoka University  
836 Ohya, Suruga-ku, Shizuoka 422-8529, Japan*

<sup>2)</sup> *Graduate School of Science and Technology, Shizuoka University  
3-5-1 Johoku, Naka-ku, Hamamatsu 432-8011, Japan*

## Abstract

We study entanglement entropy on the fuzzy sphere. We calculate it in a scalar field theory on the fuzzy sphere, which is given by a matrix model. We use a method that is based on the replica method and applicable to interacting fields as well as free fields. For free fields, we obtain the results consistent with the previous study, which serves as a test of the validity of the method. For interacting fields, we perform Monte Carlo simulations at strong coupling and see a novel behavior of entanglement entropy.

---

\* e-mail address : okuno.shizuka.14@shizuoka.ac.jp

† e-mail address : f5344003@ipc.shizuoka.ac.jp

‡ e-mail address : tsuchiya.asato@shizuoka.ac.jp

# 1 Introduction

Since the discovery of the Ryu-Takayanagi formula [1] in the context of the AdS/CFT correspondence, it has been revealed that entanglement entropy in field theory encodes the information on geometry. Because the noncommutative field theory is deeply connected to gravity and string theory, it would be worthwhile to study entanglement entropy in such field theories. Indeed, by examining a gravity dual of noncommutative Yang-Mills theory proposed in [2, 3], it was conjectured in [4, 5] that the leading contribution to entanglement entropy in noncommutative Yang-Mills theory is proportional to the volume of the focused region<sup>1</sup>, in contrast to the fact that it is proportional to the area of the boundary in ordinary field theories. This volume law is considered to originate from the UV/IR mixing [6] due to nonlocal nature of interactions. In fact, in [7], the volume law is observed in nonlocal theories.

In [8, 9]<sup>2</sup>, entanglement entropy in a scalar field theory on the fuzzy sphere, which is realized by a matrix model, was calculated for free fields<sup>3</sup>. In this paper, we are concerned with interacting fields, because the discovered UV/IR anomaly [12, 13] that is a counterpart of the UV/IR mixing in field theories on compact noncommutative manifolds arises from the interactions.

Another motivation of our work is to gain insights into connections between geometry and matrix models, which is an important subject in the context of matrix models proposed as nonperturbative formulation of string theory [14–16]. In [8, 9], the fuzzy sphere is divided into two regions using the Bloch coherent state, and correspondingly the matrices are divided into two parts. By considering the results for entanglement entropy, we should elucidate a precise geometrical meaning of this division.

In [8, 9], the method developed in [17] was used to calculate entanglement entropy. This method is valid only for free fields. In this paper, we use another method, which was developed and used in [18, 19] and can also be applied to interacting fields. We first test the validity of the method in our study by applying the method to free fields. We compare

---

<sup>1</sup> In this paper, we use terminologies ‘volume’ and ‘area’ even for sphere, although their actual meanings are area and length on sphere, respectively.

<sup>2</sup>See also [10, 11].

<sup>3</sup>In this paper, we call the case in which the action consists of only quadratic terms ‘free field’ while the case in which the action includes higher terms ‘interacting field’.

our results with those in [8, 9]. Then, we apply the method to interacting fields and perform Monte Carlo simulations<sup>4</sup>. While this work is a first step to Monte Carlo study of entanglement entropy on the fuzzy sphere, we see a novel behavior of entanglement entropy.

This paper is organized as follows. In section 2, we review a matrix model that realizes a noncommutative counterpart of a scalar field theory on  $S^1 \times S^2$ . In section 3, we describe the properties of entanglement entropy and explain the method to calculate entanglement entropy. In section 4, we show numerical results for entanglement entropy. Section 5 is devoted to discussion. In appendix A, we review the Bloch coherent state. In appendix B, the detail of the calculation in the free case is given.

## 2 Scalar field theory on the fuzzy sphere

First, we consider a scalar field theory on  $S^1 \times S^2$  defined by

$$S_C = \frac{R^2}{4\pi} \int_0^\beta dt \int d\Omega \left( \frac{1}{2} \dot{\phi}^2 - \frac{1}{2R^2} (\mathcal{L}_i \phi)^2 + \frac{\mu^2}{2} \phi^2 + \frac{\lambda}{4} \phi^4 \right), \quad (2.1)$$

where  $\beta$  is the circumference of  $S^1$  that corresponds to inverse temperature,  $R$  is the radius of  $S^2$ , the integral measure on  $S^2$  is given by  $R^2 \int d\Omega = R^2 \int_0^{2\pi} d\varphi \int_0^\pi d\theta \sin \theta$ , and the dot stands for the derivative with respect to  $t$ .  $\mathcal{L}_i$  ( $i=1,2,3$ ) are the orbital angular momentum operators that are defined by

$$\begin{aligned} \mathcal{L}_\pm &\equiv \mathcal{L}_1 \pm i\mathcal{L}_2 = e^{\pm i\varphi} \left( \pm \frac{\partial}{\partial \theta} + i \cot \theta \frac{\partial}{\partial \varphi} \right), \\ \mathcal{L}_3 &= -i \frac{\partial}{\partial \varphi}. \end{aligned} \quad (2.2)$$

A noncommutative counterpart of the theory (2.1), where  $S^2$  is replaced with the fuzzy sphere, is given by a matrix model, whose action is defined by

$$S_{NC} = \frac{R^2}{2j+1} \int_0^\beta dt \operatorname{tr} \left( \frac{1}{2} \dot{\Phi}^2 - \frac{1}{2R^2} [L_i, \Phi]^2 + \frac{\mu^2}{2} \Phi^2 + \frac{\lambda}{4} \Phi^4 \right), \quad (2.3)$$

where  $j$  is a non-negative integer or a positive half-integer, and  $\Phi$  is a  $(2j+1) \times (2j+1)$  Hermitian matrix depending on  $t$ .  $L_i$  are the generators of the  $SU(2)$  algebra with the spin  $j$  representation obeying the relation  $[L_i, L_j] = i\epsilon_{ijk} L_k$ . The theory (2.3) reduces to the theory

---

<sup>4</sup>For Monte Carlo simulations of the fuzzy sphere, see [20–25]. For analytic treatment of scalar field theory on the fuzzy sphere, see [26, 27].

(2.1) at the tree level in the limit  $j \rightarrow \infty$ , which corresponds to the continuum limit, while the theory (2.3) exhibits the UV/IR anomaly at the quantum level, which makes the theory (2.3) differ from the theory (2.1) even in the  $j \rightarrow \infty$  limit.

A simple way to see the correspondence between the two theories is to use the Bloch coherent states  $|\Omega\rangle$  ( $\Omega = (\theta, \varphi)$ ) [28]<sup>5</sup>, which are reviewed in appendix A. We identify the Berezin symbol  $f_{\Phi(t)}(\Omega) = \langle \Omega | \Phi(t) | \Omega \rangle$  [33] with  $\phi(t, \Omega)$  in the  $j \rightarrow \infty$  limit. By using (A.5), one can easily show that

$$f_{[L_i, \Phi]}(\Omega) = \mathcal{L}_i f_{\Phi}(\Omega) . \quad (2.4)$$

Moreover, for two matrices  $A$  and  $B$ , the star product is given by

$$f_A(\Omega) * f_B(\Omega) \equiv f_{AB}(\Omega) = \frac{2j+1}{4\pi} \int d\Omega' \langle \Omega | A | \Omega' \rangle \langle \Omega' | B | \Omega \rangle , \quad (2.5)$$

where we used (A.8). The star product reduces to the ordinary product at the tree level in the  $j \rightarrow \infty$  limit, while it yields the UV/IR anomaly at the quantum level. Thus the theory (2.3) reduces to the theory (2.1) at the tree level in the  $j \rightarrow \infty$  limit.

The relationship between the Berezin symbol and the matrix elements  $\langle jm | \Phi | jm' \rangle$  is given by

$$f_{\Phi}(\Omega) = \sum_{m, m'} \langle \Omega | jm \rangle \langle jm' | \Omega \rangle \langle jm | \Phi | jm' \rangle . \quad (2.6)$$

Here, by using (A.5), one finds that

$$\langle \Omega | jm \rangle \langle jm' | \Omega \rangle \sim \left( \cos \frac{\theta}{2} \right)^{2j+m+m'} \left( \sin \frac{\theta}{2} \right)^{2j-m-m'} e^{i(m-m')\varphi} , \quad (2.7)$$

which turns out to have the sharp peak at [8]

$$\cos \theta = \frac{m+m'}{2j} . \quad (2.8)$$

The width is given by  $\Delta\theta \sim \frac{1}{\sqrt{j}}$ . This implies that the matrix elements  $\langle jm | \Phi | j \ n - m \rangle$  correspond to the field  $\phi$  at  $\cos \theta = \frac{n}{2j}$  [8].

Hereafter, we put  $R = 1$  and  $\mu = 1$  for simplicity, and denote the matrix size by  $N$ , namely  $N = 2j + 1$ .

---

<sup>5</sup>See also [29–32].

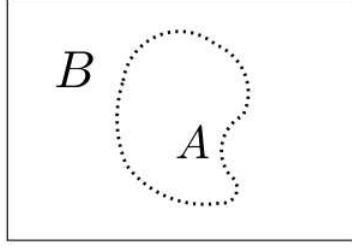


Figure 1: Region A and region B.

### 3 Calculation of entanglement entropy

In this section, we first review the properties of entanglement entropy and next explain how to calculate entanglement entropy on the fuzzy sphere.

#### 3.1 Entanglement entropy

Suppose that the Hilbert space  $\mathcal{H}$  of a system is given by a tensor product

$$\mathcal{H} = \mathcal{H}_A \otimes \mathcal{H}_B . \quad (3.1)$$

Then, the entanglement entropy  $S_A$  is defined by

$$S_A = -\text{Tr}[\rho_A \log \rho_A] . \quad (3.2)$$

Here  $\rho_A$  is obtained by taking a partial trace of the density matrix  $\rho_{tot}$  over  $\mathcal{H}_B$ :

$$\rho_A = \text{Tr}_B[\rho_{tot}] . \quad (3.3)$$

Typically, the decomposition of the Hilbert space (3.1) is realized by a decomposition of the space, on which a field theory is defined, into two regions, as the region A and the region B in Fig.1.

Entanglement entropy has the following properties. First, if the density matrix  $\rho_{tot}$  is given by a pure state, entanglement entropy satisfies

$$S_A = S_B . \quad (3.4)$$

Second, the leading contribution to the entanglement entropy  $S_A$  for the ground state in  $(d + 1)$ -dimensional local field theories ( $d \geq 2$ ) is proportional to  $|\partial A|/\epsilon^{d-1}$ , where  $|\partial A|$

is the area of the boundary between the regions A and B, and  $\epsilon$  is the UV cutoff. At finite temperature, entanglement entropy has a correction proportional to the volume of the region A. On the other hand, in nonlocal field theories, the leading contribution to the entanglement entropy  $S_A$  for the ground state can be proportional to the volume of the region A. In particular, by examining the gravity dual, it was conjectured in [4, 5] that this is indeed the case in noncommutative Yang-Mills theory.

In our study, we divide the fuzzy sphere into two region, as in [8]. By using (2.8), we identify the regions A and B on the sphere in Fig.3.1(a) with the regions A and B of the matrix  $\Phi$  in Fig.3.1(b), respectively. In order to specify the regions A and B on the sphere, we introduce a new parameter  $x$ , which is related to  $\theta$  as

$$x = 1 - \cos \theta . \quad (3.5)$$

Namely,  $x$  is the area of the region A divided by  $2\pi$ . The condition that the  $(m, m')$  component of the matrix  $\Phi$  is located in the region A is given by

$$m + m' > 2j - u , \quad (3.6)$$

where  $u = 0, 1, 2, \dots, 4j$ . Then, it follows from (2.8), (3.5) and (3.6) that the relation between  $x$  and  $u$  is given by

$$x = \frac{u}{2j} . \quad (3.7)$$

## 3.2 Replica method

In this subsection, we describe the method to calculate entanglement entropy developed in [18]. In calculating entanglement entropy, we use the replica method, in which the definition of entanglement entropy (3.2) is rewritten as

$$S_A = \lim_{\alpha \rightarrow 1} \left[ -\frac{\partial}{\partial \alpha} \text{Tr} \rho_A^\alpha \right] = \lim_{\alpha \rightarrow 1} \left[ -\frac{\partial}{\partial \alpha} \log(\text{Tr} \rho_A^\alpha) \right] , \quad (3.8)$$

where  $\alpha$  corresponds to the number of replicas and is analytically continued.

In (2.3), we yield  $\alpha$  replicas for  $\Phi(t)$ , which are denoted by  $\Phi_n(t)$  ( $n = 1, \dots, \alpha$ ). We impose the following boundary condition on  $\Phi_n(t)$  (see Fig.3):

$$\begin{aligned} \Phi_n(\beta, m, m') &= \Phi_{n+1}(0, m, m') \text{ for the region A ,} \\ \Phi_n(\beta, m, m') &= \Phi_n(0, m, m') \text{ for the region B ,} \end{aligned} \quad (3.9)$$

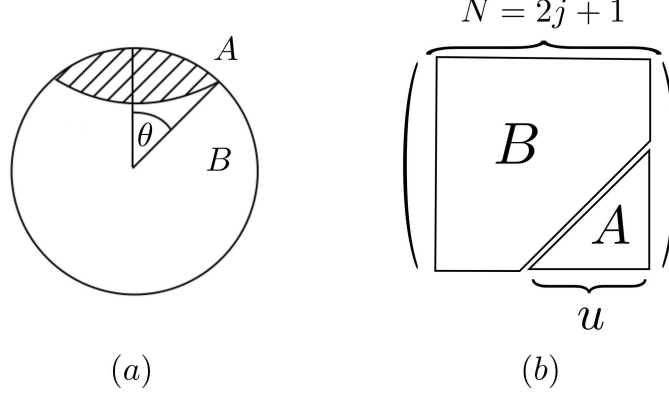


Figure 2: Correspondence of two regions on the fuzzy sphere and in the matrix model.

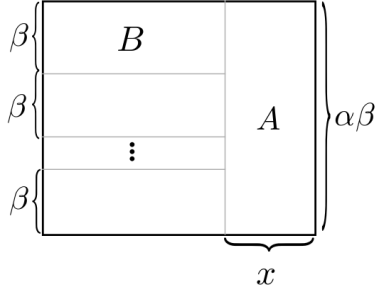


Figure 3: Replica method.

where  $n = 1, \dots, \alpha$  and  $\alpha + 1$  is identified with 1 in the first line. Then, we obtain a relation

$$\text{Tr} \rho_A^\alpha = \frac{Z(x, \alpha)}{Z^\alpha} , \quad (3.10)$$

where  $Z$  represents  $Z(\alpha = 1)$  that is independent of  $x$ . Substituting (3.10) into (3.8) leads to an expression for  $S_A$

$$S_A(x) = - \lim_{\alpha \rightarrow 1} \frac{\partial}{\partial \alpha} \ln \left( \frac{Z(x, \alpha)}{Z^\alpha} \right) . \quad (3.11)$$

We obtain entanglement entropy for the ground state in the  $\beta \rightarrow \infty$  limit, while one including finite temperature effect at finite  $\beta$ .

It is convenient to consider the derivative of  $S_A$  with respect to  $x$  instead of  $S_A$  itself:

$$\frac{\partial S_A(x)}{\partial x} = \frac{\partial}{\partial x} \left[ - \lim_{\alpha \rightarrow 1} \frac{\partial}{\partial \alpha} \ln \left( \frac{Z(x, \alpha)}{Z^\alpha} \right) \right] = \lim_{\alpha \rightarrow 1} \frac{\partial}{\partial x} \frac{\partial}{\partial \alpha} F[x, \alpha] , \quad (3.12)$$

where  $F[x, \alpha]$  is the free energy of the system Fig. 3. Here we make an approximation<sup>6</sup> for the derivative with respect to  $\alpha$  as

$$\begin{aligned} \lim_{\alpha \rightarrow 1} \frac{\partial}{\partial x} \frac{\partial}{\partial \alpha} F[x, \alpha] \\ \rightarrow \frac{\partial}{\partial x} (F[x, \alpha = 2] - F[x, \alpha = 1]) = \lim_{j \rightarrow \infty} \frac{F[x + \varepsilon, \alpha = 2] - F[x, \alpha = 2]}{\varepsilon}, \end{aligned} \quad (3.13)$$

where  $\varepsilon = \frac{1}{2^j}$ . In the next section, we test the validity of this approximation by comparing our results for free fields with those in [8,9]. Note that (3.4) implies that in the  $\beta \rightarrow \infty$  limit

$$\begin{aligned} S_A(x) &= S_A(2 - x), \\ \frac{\partial S_A}{\partial x}(x) &= -\frac{\partial S_A}{\partial x}(2 - x), \end{aligned} \quad (3.14)$$

which reflect the symmetry under  $\theta \rightarrow \pi - \theta$ .

In the case of free fields where  $\lambda = 0$ , we calculate  $F[x, \alpha = 2]$  directly by evaluating numerically the determinant that is given in appendix B.

In the case of interacting fields where  $\lambda \neq 0$ , it is convenient to introduce an interpolating action  $S_{int} = (1 - \gamma)S_{x+\varepsilon} + \gamma S_x$ , where  $S_{x+\varepsilon}$  and  $S_x$  are the actions that would yield  $F[x + \varepsilon, \alpha = 2]$  and  $F[x, \alpha = 2]$ , respectively. Then the numerator of the last expression in (3.13) can be evaluated as

$$F[x + \varepsilon, \alpha = 2] - F[x, \alpha = 2] = \int_0^1 d\gamma \langle S_{x+\varepsilon} - S_x \rangle_\gamma, \quad (3.15)$$

where  $\langle \cdots \rangle_\gamma$  stands for the expectation value with respect to the canonical weight  $e^{-S_{int}}$ . In practice, we take  $\gamma$  from 0 to 1 by the step 0.1, and calculate  $\langle S_{x+\varepsilon} - S_x \rangle_\gamma$  for each  $\gamma$ . We finally use the Simpson formula for the integral to obtain the right-hand side of (3.15).

In both cases, we introduce the lattice in the time direction and denote the lattice spacing by  $a$ .

## 4 Results

In this section, we show our results for free fields ( $\lambda = 0$ ) and for interacting fields. In the latter case, we put  $\lambda = 1.0$ , which would correspond to a strong coupling.

---

<sup>6</sup> Precisely speaking, we calculate the derivative of the Rényi entropy with the Rényi parameter equal to two with respect to  $x$ .



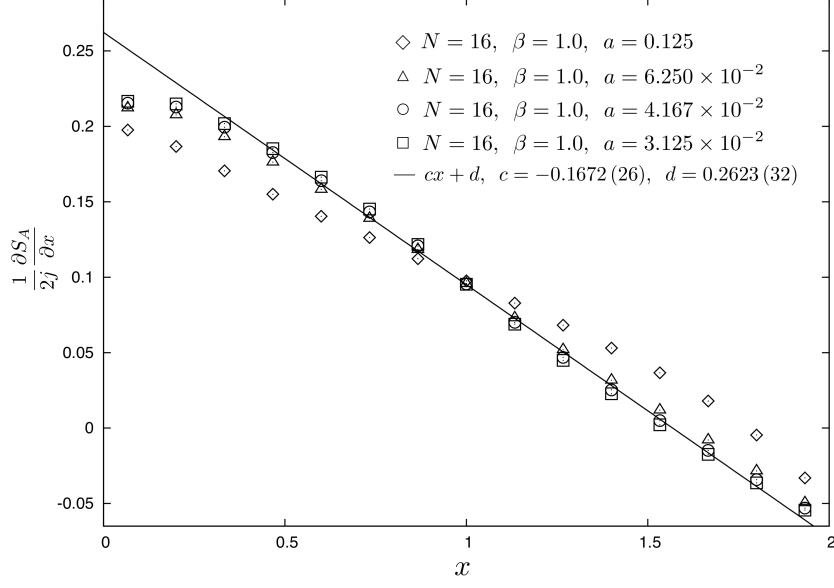


Figure 4: The derivative of entanglement entropy with respect to  $x$  divided by  $2j$  is plotted against  $x$  at  $\lambda = 0$ ,  $N = 16$  and  $\beta = 1.0$ . The diamonds, the triangles, the circles and the squares represent the data for  $a = 0.125, 6.250 \times 10^{-2}, 4.167 \times 10^{-2}, 3.125 \times 10^{-2}$ , respectively. The solid line is a fit of the data for  $a = 3.125 \times 10^{-2}$  to  $\frac{1}{2j} \frac{\partial S_A}{\partial x} = cx + d$  for  $0.333 \leq x \leq 1.800$ , which gives  $c = -0.1672(26)$  and  $d = 0.2623(32)$ .

#### 4.1 $\lambda = 0$

We first calculate  $F[x, \alpha = 2]$  numerically by the method given in appendix B and then calculate the derivative of the entanglement entropy  $S_A$  with respect to  $x$  following (3.13). The derivative of  $S_A$  with respect to  $x$  divided by  $2j$  is plotted against  $x$  in Fig. 4 - Fig. 6.

We observe that at  $\beta = 1.0$  the data for odd  $u$  exhibits a smooth behavior while the data for even  $u$  exhibits another smooth behavior (note that  $x = \frac{u}{2j}$ ). This discrepancy almost disappears at  $\beta = 4.0$ . This discrepancy is considered to come from a finite  $N$  effect that becomes stronger at high temperature. Indeed, as we will see shortly, the continuum limit in the time direction can be taken at  $\beta = 1.0$  using only the data for odd  $u$  or even  $u$  (see Fig. 4 for odd  $u$  at  $\beta = 1.0$  and Fig. 5 for odd  $u$  at  $\beta = 3.0$ ), so that the two continuum limits for odd  $u$  and for even  $u$  differ only by finite temperature effect. Because we are concerned with the part except the finite temperature effect, we plot only the data for odd  $u$  in the following.

In Fig. 4 and Fig. 5, we examine the continuum limit in the time direction at  $N = 16$  and  $\beta = 1.0$  and at  $N = 16$  and  $\beta = 3.0$ , respectively. We plot the data for four different values of the lattice spacing  $a$ . We observe that the continuum limit is taken, and  $a = 4.167 \times 10^{-2}$  is close enough to the continuum limit. The data for  $a = 3.125 \times 10^{-2}$  is fitted to the linear function  $\frac{1}{2j} \frac{\partial S_A}{\partial x} = cx + d$ , where we exclude some data points around  $x = 0$  and  $x = 2.0$ , where the area of the region A or the region B is small so that ambiguity of the boundary between the two regions due to finite  $N$  effect is relevant. We use the range  $0.333 \leq x \leq 1.8$  for  $\beta = 1.0$  and the range  $0.2 \leq x \leq 1.8$  for  $\beta = 3.0$ . We obtain  $c = -0.1672(26)$  and  $d = 0.2623(32)$  for  $\beta = 1.0$  and  $c = -0.1612(29)$  and  $d = 0.1629(33)$  for  $\beta = 3.0$ .

In Fig. 5, we also plot the data for  $N = 16$ ,  $\beta = 4.0$  and  $a = 4.167 \times 10^{-2}$ . We see that the data almost agree with those for  $N = 16$ ,  $\beta = 3.0$  and  $a = 4.167 \times 10^{-2}$ . This implies that the low temperature limit (the  $\beta \rightarrow \infty$  limit) is taken and that  $\beta = 3.0$  is close enough to the low temperature limit. Indeed, the function  $\frac{1}{2j} \frac{\partial S_A}{\partial x} = cx + d$  with  $c = -0.1612(29)$  and  $d = 0.1629(33)$  to which the data for  $N = 16$ ,  $\beta = 3.0$  and  $a = 3.125 \times 10^{-2}$  are fitted is consistent with (3.14). Namely, the function is proportional to  $1 - x$  within the fitting error. This implies that

$$S_A \propto 2x - x^2 = \sin^2 \theta . \quad (4.1)$$

This behavior agrees with the one observed in [8, 9] up to an overall coefficient.

By comparing the above values of  $c$  and  $d$  obtained in the fitting of the data for  $\beta = 1.0$  with those obtained in the fitting of the data for  $\beta = 3.0$ , we see that the difference of the two functions  $\frac{1}{2j} \frac{\partial S_A}{\partial x} = cx + d$  is almost constant. This implies that the finite temperature contribution to entanglement entropy is proportional to  $x$ , namely the volume of the region A. This is a general property of entanglement entropy. We also fit the data with even  $u$  for  $N = 16$ ,  $\beta = 1.0$  and  $a = 3.125 \times 10^{-2}$  to  $\frac{1}{2j} \frac{\partial S_A}{\partial x} = cx + d$  for  $0.133 \leq x \leq 1.6$  and obtain  $c = 0.1626(26)$  and  $d = 0.2690(22)$ . As we stated, the difference between the fitting of the data with odd  $u$  and the one of the data with even  $u$  is almost constant, which is finite temperature effect.

In Fig. 6, we examine the large- $N$  (large- $j$ ) limit. At  $\beta = 1.0$  and  $a = 4.167 \times 10^{-2}$ , we plot the data for  $N = 16, 24, 32$ . We observe that the data converge as  $N$  increases. This implies that entanglement entropy scales as  $N$ , which is consistent with the observation in [8, 9]. We fit the data for  $N = 32$  to the function  $\frac{1}{2j} \frac{\partial S_A}{\partial x} = cx + d$  for  $0.0967 \leq x \leq 1.903$

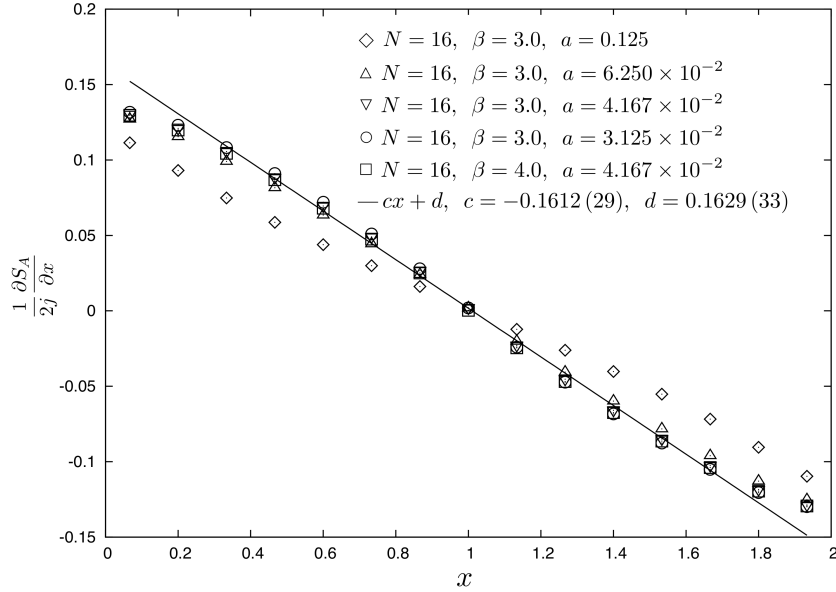


Figure 5: The derivative of entanglement entropy with respect to  $x$  divided by  $2j$  is plotted against  $x$  at  $\lambda = 0$  and  $N = 16$ . The diamonds, the triangles, the inverted triangles and the circles represent the data for  $\beta = 3.0$  and  $a = 0.125, 6.250 \times 10^{-2}, 4.167 \times 10^{-2}, 3.125 \times 10^{-2}$ , respectively, while the squares represent the data for  $\beta = 4.0$  and  $a = 4.167 \times 10^{-2}$ . The solid line is a fit of the data for  $\beta = 3.0$  and  $a = 3.125 \times 10^{-2}$  to  $\frac{1}{2j} \frac{\partial S_A}{\partial x} = cx + d$  for  $0.200 \leq x \leq 1.800$ , which gives  $c = -0.1612(29)$  and  $d = 0.1629(33)$ .

and obtain  $c = -0.1509(8)$  and  $d = 0.1962(9)$ . Thus, our method is valid in the sense that it reproduces the  $\theta$  dependence (4.1) and the  $N$  dependence of entanglement entropy precisely.

## 4.2 $\lambda = 1.0$

In this subsection, we study the case of  $\lambda = 1.0$ . In the previous subsection, we saw in the case of  $\lambda = 0$  that the finite temperature effect is controllable. Thus, as a first step, we decide to perform Monte Carlo simulations at  $N = 16$ ,  $\beta = 1.0$  and  $a = 0.125$  taking into account the computation time.

We use the Hybrid Monte Carlo method and make 3,000,000 trajectories for each  $\gamma = 0.0, 0.1, \dots, 1.0$ , discarding the first 100,000 trajectories for the thermalization.

In Fig. 7, we plot the derivative of entanglement entropy with respect to  $x$  divided by  $2j$  against  $x$ . We again observe the discrepancy between odd  $u$  and even  $u$  similar to the case of  $\lambda = 0$ , so that we plot only the data for odd  $u$ . We see that the data can be shifted

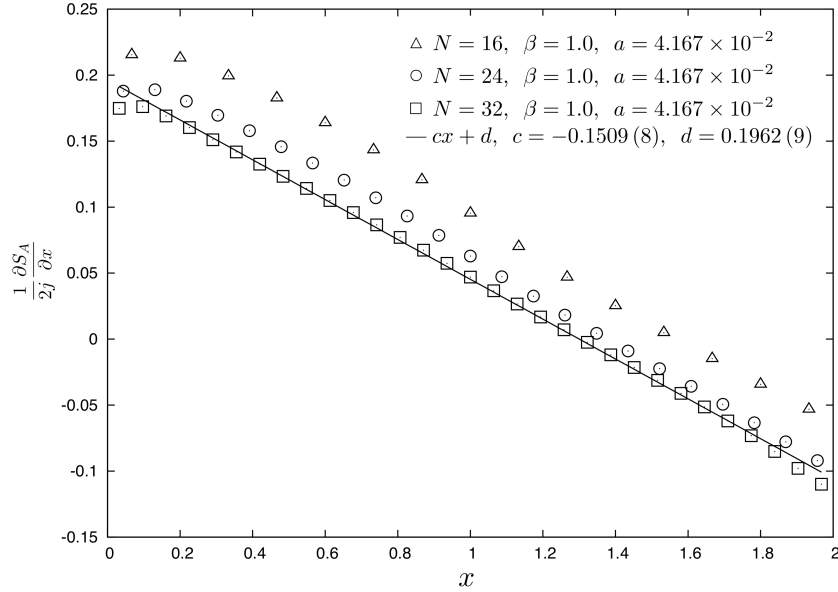


Figure 6: The derivative of entanglement entropy with respect to  $x$  divided by  $2j$  is plotted against  $x$  at  $\lambda = 0$ ,  $\beta = 1.0$  and  $a = 4.167 \times 10^{-2}$ . The triangles, the circles and the squares represent the data for  $N = 16, 24, 32$ , respectively. The solid line is a fit of the data for  $N = 32$  to  $\frac{1}{2j} \frac{\partial S_A}{\partial x} = cx + d$  for  $9.677 \times 10^{-2} \leq x \leq 1.903$ , which gives  $c = -0.1509(8)$  and  $d = 0.1962(9)$ .

by a constant in the vertical direction in such a way that they are consistent with (3.14) except  $u = 13, 15, 17$ . Thus, we conjecture that also in the case of interacting fields the finite temperature effect in entanglement entropy is also proportional to the volume of the region A as in the case of free fields. Comparing Fig. 7 with Fig. 4, we also see that the data for  $\lambda = 1.0$  behave in a clearly different way from the data for  $\lambda = 0$  with the same values of  $N$ ,  $\beta$  and  $a$ . Indeed, while the data for  $\lambda = 0$  can be fitted to  $\frac{1}{2j} \frac{\partial S_A}{\partial x} = cx + d$  with  $c = -0.1276(33)$  and  $d = 0.2140(37)$  for  $0.2 \leq x \leq 1.933$ , while the data for  $\lambda = 1.0$  cannot be fitted to such a linear function. Furthermore, the magnitude of entanglement entropy for  $\lambda = 0$  is about ten times larger than that for  $\lambda = 1.0$ . We conjecture that this drastic difference is attributed to nonlocal interactions as well as strong coupling.

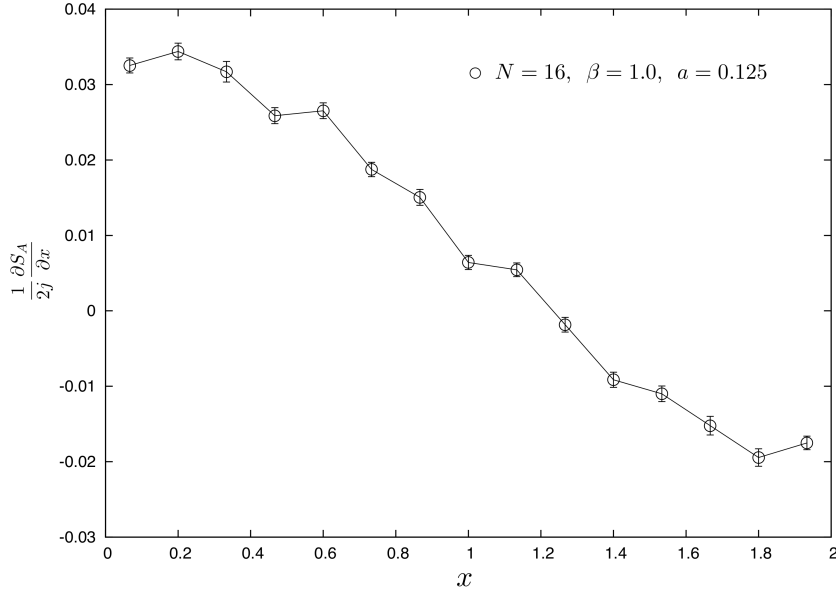


Figure 7: The derivative of entanglement entropy with respect to  $x$  divided by  $2j$  is plotted against  $x$  at  $\lambda = 1.0$ ,  $N = 16$ ,  $\beta = 1.0$  and  $a = 0.125$ .

## 5 Discussion

In this paper, we calculated entanglement entropy in the scalar field theory on the fuzzy sphere. We use the method developed and used in [18,19]. In the case of  $\lambda = 0$ , we obtained the results that are consistent with those in [8,9]. This serves as a check of the validity of the method in our study. We performed Monte Carlo simulations to calculate entanglement entropy at strong coupling ( $\lambda = 1.0$ ). This is the first result for interacting fields on the fuzzy sphere.

We found in the case of free fields that the finite temperature effect in entanglement entropy is proportional to the volume of the focused region as in ordinary field theories. We conjecture from the result of Monte Carlo simulations that the same is true for the case of interacting fields. We saw that the behavior of entanglement entropy for interacting fields is clearly different from that for free fields. In particular, we found that magnitude of entanglement entropy for free fields is about ten times larger than that for interacting fields. We conjecture that this drastic difference is attributed to nonlocal interactions as well as strong coupling.

For free fields, we confirmed the observation in [8, 9] that the entanglement entropy for the ground state is proportional to the square of the area of the boundary ( $\sim \sin^2 \theta$ ) and scales as  $N$ . For interacting fields, we should examine the continuum limit and establish the  $\theta$  dependence of entanglement entropy, which is naively expected to be proportional to the volume. We should give a physical interpretation on the behavior of entanglement entropy for interacting fields as well as for free fields. We would also like to study the  $\lambda$  dependence of entanglement entropy. In particular, we are interested in whether there exists a phase transition or not. By continuing Monte Carlo simulations, we hope to report on the above issues in the near future.

## Acknowledgements

We would like to thank G. Ishiki and E. Itou for discussions. Numerical computation was carried out on SR16000 at YITP in Kyoto University and SR16000 at University of Tokyo. The work of A.T. is supported in part by Grant-in-Aid for Scientific Research (No. 24540264, 23244057 and 15K05046) from JSPS.

## Appendix A: Bloch coherent states

In this appendix, we review the Bloch coherent state [28]. We introduce a standard basis  $|jm\rangle$  ( $m = -j, -j+1, \dots, j$ ) for the spin  $j$  representation of the  $SU(2)$  algebra, which obey the relations

$$\begin{aligned} L_{\pm}|jm\rangle &= \sqrt{(j \mp m)(j \pm m + 1)}|jm \pm 1\rangle, \\ L_3|jm\rangle &= m|jm\rangle, \end{aligned} \tag{A.1}$$

where  $L_{\pm} = L_1 \pm iL_2$ . We consider the state  $|jj\rangle$  to correspond to the north pole on unit sphere. Then, the state  $|\Omega\rangle$  that corresponds to a point  $\Omega = (\theta, \varphi)$  on unit sphere is obtained by multiplying  $|jj\rangle$  by a rotation operator:

$$|\Omega\rangle = e^{i\theta(\sin \varphi L_1 - \cos \varphi L_2)}|jj\rangle, \tag{A.2}$$

from which it follows that

$$n_i L_i |\Omega\rangle = j |\Omega\rangle, \tag{A.3}$$

where  $\vec{n} = (\sin \theta \cos \varphi, \sin \theta \sin \varphi, \cos \theta)$ . This implies that the states  $|\Omega\rangle$  minimize  $\sum_i (\Delta L_i)^2$ , where  $(\Delta L_i)^2$  is the standard deviation of  $L_i$ . The states  $|\Omega\rangle$  are called the Bloch coherent states. (A.2) is rewritten as

$$|\Omega\rangle = e^{zL_-} e^{-L_3 \log(1+|z|^2)} e^{-\bar{z}L_+} |jj\rangle, \quad (\text{A.4})$$

where  $z = \tan \frac{\theta}{2} e^{i\varphi}$ . An explicit form of  $|\Omega\rangle$  is obtained from (A.4) as

$$|\Omega\rangle = \sum_{m=-j}^j \binom{2j}{j+m}^{\frac{1}{2}} \left( \cos \frac{\theta}{2} \right)^{j+m} \left( \sin \frac{\theta}{2} \right)^{j-m} e^{i(j-m)\varphi} |jm\rangle. \quad (\text{A.5})$$

It is easy to show the following relations by using (A.5):

$$\langle \Omega_1 | \Omega_2 \rangle = \left( \cos \frac{\theta_1}{2} \cos \frac{\theta_2}{2} + e^{i(\varphi_2 - \varphi_1)} \sin \frac{\theta_1}{2} \sin \frac{\theta_2}{2} \right)^{2j}, \quad (\text{A.6})$$

$$|\langle \Omega_1 | \Omega_2 \rangle| = \left( \cos \frac{\chi}{2} \right)^{2j} \quad \text{with } \chi = \arccos(\vec{n}_1 \cdot \vec{n}_2), \quad (\text{A.7})$$

$$\frac{2j+1}{4\pi} \int d\Omega |\Omega\rangle \langle \Omega| = 1. \quad (\text{A.8})$$

Putting  $\chi = \frac{2}{\sqrt{j}}$  in the the right-hand side of (A.7) gives rise to

$$\left( \cos \frac{\chi}{2} \right)^{2j} \approx \left( 1 - \frac{1}{2j} \right)^{2j} \approx e^{-1} \quad (\text{A.9})$$

for large  $j$ . This implies that the effective width of the Bloch coherent state is proportional to  $\frac{R}{\sqrt{j}}$ .

## Appendix B: The action with $\lambda = 0$

In this appendix, we describe how to calculate  $F[x, \alpha = 2]$  in the case of free fields. We extend the length of the time direction from  $\beta$  to  $2\beta$  and divide it into  $2M$  sites, so that the lattice spacing  $a$  is  $a = \frac{\beta}{M}$ . We unify  $\Phi_1$  and  $\Phi_2$  into  $\Phi(n)$  ( $n = 1, 2, \dots, 2M$ ) such that  $\Phi(n) = \Phi_1(na)$  for  $n = 1, \dots, M$  and  $\Phi(n) = \Phi_2((n-M)a)$  for  $n = M+1, \dots, 2M$ . Then,

the discretized action with  $\lambda = 0$  is

$$\begin{aligned}
S_{NC} = & \frac{a}{2} \left[ \sum_{m+m' \leq 2j-u} \left\{ \sum_{n=1}^{M-1} \left| \frac{\Phi_{mm'}(n+1) - \Phi_{mm'}(n)}{a} \right|^2 + \left| \frac{\Phi_{mm'}(1) - \Phi_{mm'}(M)}{a} \right|^2 \right. \right. \\
& + \sum_{n=M+1}^{2M-1} \left| \frac{\Phi_{mm'}(n+1) - \Phi_{mm'}(n)}{a} \right|^2 + \left| \frac{\Phi_{mm'}(M+1) - \Phi_{mm'}(2M)}{a} \right|^2 \Big\} \\
& + \sum_{m+m' > 2j-u} \left\{ \sum_{n=1}^{2M-1} \left| \frac{\Phi_{mm'}(n+1) - \Phi_{mm'}(n)}{a} \right|^2 + \left| \frac{\Phi_{mm'}(1) - \Phi_{mm'}(2M)}{a} \right|^2 \right\} \\
& \left. + \sum_{mm'} \sum_{n=1}^{2M} \left\{ \Phi_{mm'}(n) [L_i, [L_i, \Phi(n)]]_{m'm} + m^2 |\Phi_{mm'}(n)|^2 \right\} \right] . \tag{B.1}
\end{aligned}$$

Here we introduce a matrix  $T_{nij,mkl}$  that is defined by

$$S_{NC} = \sum_{n,l,m_1,m_2,m_3,m_4} \Phi_{m_1 m_2}^*(n) T_{nm_1 m_2, lm_3 m_4} \Phi_{m_3 m_4}(l) . \tag{B.2}$$

We read off the matrix  $T$  from (B.1) and calculate its determinant numerically. Then, the free energy is given by

$$F[x, \alpha = 2] = \frac{1}{2} \log \det T + \text{const.} . \tag{B.3}$$

The constant in the right-hand side does not contribute to the derivative of entanglement entropy with respect to  $x$ .

## References

- [1] S. Ryu and T. Takayanagi, Phys. Rev. Lett. **96**, 181602 (2006) [hep-th/0603001].
- [2] A. Hashimoto and N. Itzhaki, Phys. Lett. B **465**, 142 (1999) [hep-th/9907166].
- [3] J. M. Maldacena and J. G. Russo, JHEP **9909**, 025 (1999) [hep-th/9908134].
- [4] W. Fischler, A. Kundu and S. Kundu, JHEP **1401**, 137 (2014) [arXiv:1307.2932 [hep-th]].
- [5] J. L. Karczmarek and C. Rabideau, JHEP **1310**, 078 (2013) [arXiv:1307.3517 [hep-th]].
- [6] S. Minwalla, M. Van Raamsdonk and N. Seiberg, JHEP **0002**, 020 (2000) [hep-th/9912072].



- [7] N. Shiba and T. Takayanagi, JHEP **1402**, 033 (2014) [arXiv:1311.1643 [hep-th]].
- [8] J. L. Karczmarek and P. Sabella-Garnier, JHEP **1403**, 129 (2014) [arXiv:1310.8345 [hep-th]].
- [9] P. Sabella-Garnier, JHEP **1502**, 063 (2015) [arXiv:1409.7069 [hep-th]].
- [10] D. Dou and B. Ydri, Phys. Rev. D **74**, 044014 (2006) [gr-qc/0605003].
- [11] D. Dou, Mod. Phys. Lett. A **24**, 2467 (2009) [arXiv:0903.3731 [gr-qc]].
- [12] C. S. Chu, J. Madore and H. Steinacker, JHEP **0108**, 038 (2001) [hep-th/0106205].
- [13] P. Castro-Villarreal, R. Delgadillo-Blando and B. Ydri, Nucl. Phys. B **704**, 111 (2005) [hep-th/0405201].
- [14] T. Banks, W. Fischler, S. H. Shenker and L. Susskind, Phys. Rev. D **55**, 5112 (1997) [hep-th/9610043].
- [15] N. Ishibashi, H. Kawai, Y. Kitazawa and A. Tsuchiya, Nucl. Phys. B **498**, 467 (1997) [hep-th/9612115].
- [16] R. Dijkgraaf, E. P. Verlinde and H. L. Verlinde, Nucl. Phys. B **500**, 43 (1997) [hep-th/9703030].
- [17] M. Srednicki, Phys. Rev. Lett. **71**, 666 (1993) [hep-th/9303048].
- [18] P. V. Buividovich and M. I. Polikarpov, Nucl. Phys. B **802**, 458 (2008) [arXiv:0802.4247 [hep-lat]].
- [19] Y. Nakagawa, A. Nakamura, S. Motoki and V. I. Zakharov, PoS LATTICE **2010**, 281 (2010) [arXiv:1104.1011 [hep-lat]].
- [20] T. Azuma, S. Bal, K. Nagao and J. Nishimura, JHEP **0405**, 005 (2004) [hep-th/0401038].
- [21] T. Azuma, S. Bal and J. Nishimura, Phys. Rev. D **72**, 066005 (2005) [hep-th/0504217].
- [22] J. Medina, W. Bietenholz, F. Hofheinz and D. O'Connor, PoS LAT **2005**, 263 (2006) [hep-lat/0509162].

- [23] F. Garcia Flores, X. Martin and D. O'Connor, Int. J. Mod. Phys. A **24**, 3917 (2009) [arXiv:0903.1986 [hep-lat]].
- [24] M. Panero, JHEP **0705**, 082 (2007) [hep-th/0608202].
- [25] C. R. Das, S. Digal and T. R. Govindarajan, Mod. Phys. Lett. A **23**, 1781 (2008) [arXiv:0706.0695 [hep-th]].
- [26] H. Steinacker, Nucl. Phys. B **679**, 66 (2004) [hep-th/0307075].
- [27] S. Kawamoto and T. Kuroki, JHEP **1506**, 062 (2015) [arXiv:1503.08411 [hep-th]].
- [28] J. P. Gazeau. Coherent states in quantum physics - 2009. Weinheim, Germany: WileyVCH.
- [29] G. Alexanian, A. Pinzul and A. Stern, Nucl. Phys. B **600**, 531 (2001) [hep-th/0010187].
- [30] A. B. Hammou, M. Lagraa and M. M. Sheikh-Jabbari, Phys. Rev. D **66**, 025025 (2002) [hep-th/0110291].
- [31] P. Presnajder, J. Math. Phys. **41**, 2789 (2000) [hep-th/9912050].
- [32] G. Ishiki, Phys. Rev. D **92**, no. 4, 046009 (2015) [arXiv:1503.01230 [hep-th]].
- [33] F. A. Berezin, Commun. Math. Phys. **40**, 153 (1975).